University of Tartu
Faculty of Science and Technology
Institute of Technology

Aleksander Parelo

Development of ESTCube-2 side panels

Bachelor thesis (12 EAP)

Computer engineering

Supervisors:

Hendrik Ehrpais, MSc

Erik Ilbis, MSc

Tartu 2018

Abstract

This thesis covers the design of ESTCube-2 nanosatellite sidepanels, the thesis focuses mainly on the design and testing of two side panel components: Sun sensors and magnetorquers. Rest of the side panel design is covered in less detail. The main goals of this work are to develop and test the magnetorquer electronics, the magnetic coils and to develop software for and test the Sun sensor.

In this work an overview of ESTCube-2 and the side panels is given, then side panel requirements are set. Based on these requirements two modules for the side panels are developed and tested.

The Sun sensors requirements are set, then a prototype sensor is presented that is based on these requirements. The software is developed, and the prototype sensor is tested in an optics laboratory to verify that they meet the requirements.

Requirements are set for the coils and the coil driving electronics and designs are developed based on these requirements. The magnetorquers are tested to verify the designs.

Keywords: ESTCube-2, side panels, electronics, Sun sensor, magnetorquer

CERCS: T170 electronics, T320 Space technology

Resümee

Käesolev lõputöö käsitleb ESTCube-2 nanosatelliidi külgpaneelide disaini. Lõputöös keskendutakse peamiselt kahe külgpaneeli mooduli disainile ja testimisele, nendeks mooduliteks on päikesesensorid ja magnettõukurid. Töö peamisteks eesmärkideks on päikesesensori prototüübile tarkvara arendamine ja arendatud tarkvara testimine. Lisaks magnettõukurite mähiste ja elektroonika arendamine ning seejärel testimine.

Töös antakse ülevaade ESTCube-2st ja selle külgpaneelidest. Seejärel seatakse külgpaneelide nõuded ja kirjeldatakse nende nõuete põhjal disainitud kahte külgpaneelidel olevat moodulit.

Päikesesensorite kohta antakse ülevaade nõudmistest ja nende nõudmiste põhjal loodud disainist. Seejärel kirjeldatakse arendatud tarkvara ja päikesesensori testimist optikalaboris.

Magnettõukurite jaoks pannakse paika disaininõuded poolidele ja juhtelektroonikale, seejärel kirjeldatakse nende nõudmiste põhjal loodud disaine ja nende disainide testimist.

Märksõnad: ESTCube-2, küljepaneelid, elektroonika, päikesesensorid, magnettõukurid

CERCS: T170 elektroonika, T320 kosmosetehnoloogia

Table of Contents

List of Figures

List of Tables

Abbreviations

ADC – analog to digital converter

AOCS – Attitude and orbit control system

COM – Communications module

COTS – commercial off the self

DMA – direct memory access

EOS – end-of-signal

EPS – Electrical power system

FOV – field-of-view

FRAM – ferroelectric random-access memory

IC – integrated circuit

ICP – internal communication protocol

LED – light emitting diode

MCU – Microcontroller unit

MPPT – Maximum power point tracking

OBC – on-board computer

OBCS – On-board computer system

PCB – printed circuit board

PSD – position sensitive device

PWM – pulse-width modulation

RAM – random access memory

SPI – serial peripheral interface

UART – Universal asynchronous receiver-transmitter

1 Introduction

Side panels are an important part of a nanosatellite, they allow the space in the sides of the satellite to be utilized for sensors and actuators that would otherwise have to be placed in the main bus, which holds all the other satellite electronics. By moving some of the components to the side panels, the main bus can be made more compact which leaves more room for payloads.

This thesis covers the design of the side panel electronics of ESTCube-2 nanosatellite. There will be a total of six side panels that are placed on the sides of the satellite and will house different sensors and actuators. Since the side panels are very similar in functionality the design is divided into smaller modules that can be placed on the side panels as required. There is a total of 6 modules.

This thesis will focus mainly on the development of two of these modules, magnetorquers and Sun sensors. The other modules are described in less detail since those have already been designed and are ready to be implemented into the side panels.

The objective of this thesis is to describe the requirements for the coil driver and Sun sensor electronics and design the electronics for the coil driver. Sun sensor software is also developed, and preliminary testing of Sun sensors is carried out.

The thesis is divided into four chapters. Chapter 2 gives a short overview of CubeSats and ESTCube-2. Chapter 3 talks about side panels in general and gives an overview of the requirements and design of the side panels. Chapter 4 talks about Sun sensors, an overview of a Sun sensor is given, the design of the ESTCube-2 Sun sensor is presented and initial test results are presented. Chapter 5 talks about magnetorquers, a general overview of magnetic torque is given, and the design of the coil driver is presented.

2 Overview

2.1 Overview of CubeSats

The CubeSat standard was developed at the California Polytechnic State University in 1999, the standard defines a common size for nanosatellites to increase accessibility to space. A standard 1U CubeSat is 10x10x11.3 cm in size and has a maximum weight of 1.3 kg. These units can be stacked to create larger CubeSats, currently CubeSats up to 12U are being built. [1]

2.2 Overview of ESTCube-2

ESTCube-2 is a 3U (10x10x34.5 cm) CubeSat being developed mostly by students at the University of Tartu in collaboration with students from other universities. The payloads are developed in cooperation with Finnish Meteorological Institute, Ventspils University College, NanoSpace AB, University of Tartu and Estsat OÜ. The satellite builds on the successful ESTCube-1 satellite. [2]

Figure 1: ESTCube-2 artist impression by Taavi Torim

The satellite is different from most other satellites that use a modular approach [2] [3] [4] as it has an integrated satellite platform that is as compact as possible which leaves more room for payloads. The entire satellite bus will be only 0.5 U in size, that includes the on-board computer (OBC), electrical power system (EPS), the attitude and orbit control system (AOCS) and the communications module (COM). [5] The sidepanels that are the focus of this thesis complement this design approach by offloading some of the components from the main subsystems. This saves volume that can be used for other systems by taking advantage of the extra space that is allowed by various CubeSat deployers. [6]

The main mission of the satellite is to test the electric solar wind sail for deorbiting. In addition to the electric solar wind sail, the satellite will also have an earth observation payload, a corrosion resistant coating experiment, an experimental cold gas thruster module and a high-speed communications module. [7]

3 Side panels

3.1 Overview of other side panels

Currently most of the side panels in use on nanosatellites are not intelligent and connect the actuators and sensors on the side panels directly to the main bus. This design requires more pins on the main OBC MCU for side panel connections, which means that more wires need to be run from the side panels to the main bus.

Most side panels have similar designs, featuring solar panels, sun sensors and magnetorquers as these components need to be placed on the outside of the satellite for proper operation. [8]

ESTCube-2 will have intelligent side panels which use their own low power MCUs to collect and preprocess the data before sending it to the OBC using the ICP protocol that requires only four wires for data transmission.

3.2 Overview of ESTCube-2 side panels

Side panels are made of aluminum and placed on the side of the satellite. One side of the side panel is covered in solar cells that are separated from the aluminum by a dielectric layer and held in place using adhesive, the other side has a printed circuit board (PCB) that is also held in place by an adhesive. Every side of the satellite will have a side panel, the size and shape of the side panel PCB on each side will depend on the space available on that side, which is shared with other sub-systems and payloads.

Each sidepanel will contain a microcontroller (MCU) for initial data gathering and processing, they will also have sensors and actuators for AOCS, an MPPT module for the solar panels and interfaces for payloads. The side panels communicate with OBC using the internal communication protocol (ICP) which reduces the number of connections needed from the side panels to the OBC.

Side panels have the same functional blocks, but the number and placement of these blocks varies between the side panels. Every side panel has an MCU, a magnetometer, a temperature sensor, ICP lines and an interrupt line. In addition to these common blocks there are blocks

that are present only on some of the side panels. Table 1 shows an overview of these functional blocks.

Table 1: Overview of side panel functional blocks

side	coil driver	Sun sensor	MPPT	burning mechanism	extra
X+		1	1	1	Payload UART
X-	1	1	1		
Y+	1	1	1		
Y-		1	1		
Z+		1	2	1	
Z-		2		1	

3.3 Side panel requirements

Side panel requirements are mostly set by the sub-systems that have components on the side panels. In addition to the requirements set by the various sub-systems there were also side panel specific requirements. Module specific requirements are given in the chapters below

The main side panel specific requirement is that all the side panels should be as interchangeable as possible to facilitate the development of common hardware and software as much as possible. This makes it easier to test the hardware and software of the side panels, reducing the chance of failure of the satellite.

Another side panel specific requirement is the physical size of the components which is determined by the area available inside the sides of the satellite. The size limitations are outlined in the requirements of specific modules. This requirement is fixed by the system level design of the satellite, which has been mostly finished.

The side panels also must be able to connect to the electrical power subsystem for power, the voltages available from the EPS are set by the EPS and cannot be changed. Two voltages are made available for the side panels, a regulated 3.3 V line and an unregulated battery voltage. [5] This means that the side panel components using the unregulated battery voltage need to have their own voltage regulators.

3.4 Side panel design

The side panels were designed as independent modules that will be placed on each satellite side. All the modules are self-contained and can be developed and designed independently of each other. The final design has 6 modules, which are ICP, magnetometer, magnetorquer, MPPT, MCU and Sun sensor.

This thesis focuses mostly on the Sun sensor and magnetorquer modules, Sun sensors are described in depth in chapter 4 and magnetorquers are looked at in chapter 5. The other modules are discussed briefly in the following sections of this chapter.

3.5 Side panel MCU

Each side panel has its own MCU for data collection and initial processing. The MCU is Texas Instruments MSP430FR5969. It was chosen for its low power consumption, verified performance in space and high FRAM size. At the time of the selection the MSP430FR5969 had the highest FRAM capacity available among MCUs. The chosen MCU also has the capability to use the FRAM as RAM when running at an 8 MHz clock speed. [9]

3.5.1 Internal communication protocol

The MCU is connected to the OBC using the ICP protocol. ICP uses RS485 protocol with two extra lines SHUTUP and ENABLE to communicate [10]. A LTC2850 transceiver is used to interface the MCU with ICP [11]. Each side panel will also have an interrupt line to the main OBC that can be used to generate an interrupt on the OBC.

3.6 Side panel sensors

The side panels contain various sensors: Sun sensors, a magnetometers and temperature sensors. Temperature sensors are side panels not discussed in depth as they require no special design considerations. The temperature sensors used are LMT86 analog sensors by Texas Instruments, the sensors are used to measure the temperature on the side panel which will be used for calibration.

Magnetometers for the attitude determination system have already been chosen and the same sensors will be implemented on the side panels. The selected magnetometer is LIS3MDL,

which is connected to the MCU using SPI. [12] Drivers for the magnetometer need to be written based on the implementation for a different MCU that is used on the satellite, but this was left outside the scope of this thesis.

4 Sun sensors

Sun sensors are sensors that measure the angle of the satellite with respect to the Sun. ESTCube-2 will have a total of six Sun sensors, one on each side of the satellite. This allows for continuous measurement of satellite attitude if at least one side of the satellite is facing the Sun.

4.1 Overview of other sun sensors

Sun sensors are one of the primary ways of attitude estimation on nanosatellites, as such many different designs have been developed and tested [13]. Many sun sensors of varying capabilities are also available as commercial off the shelf components (COTS) [14] [15].

Sun sensors can be divided into coarse and fine sun sensors, with coarse sun sensors having a larger FOV but lower accuracy and fine sun sensors having a smaller FOV and a higher accuracy.

Most Sun sensors are based on either a position sensitive device (PSD) or a linear image sensor. Linear image sensors are more difficult to implement and have higher power requirements but provide more data points that can be processed to get higher measurement accuracy.

One of the main challenges faced by sun sensors is the high intensity of the sun that saturates the sensors, which makes them useless [16]. High intensity can also cause the sensors to become non-linear which needs to be compensated for [17].

The main downside of COTS sun sensors is their price, which is usually much higher than the cost of developing the sun sensors in-house.

ESTCube-2 Sun sensors are developed in-house because due to the mission requirements of the satellite, the Sun sensors need work accurately even at high spin rates which means that

a high sampling speed and accurate timing of the samples is required. The proposed design is based on two 1D linear image sensors, so that the data can be processed on a low power MCU.

4.2 Design requirements

The design requirements for the Sun sensors are mostly set by the AOCS sub-system. The Sun sensors need to always be able to see the Sun when the satellite is not in Earths' shadow, this means that all sides of the satellite need to have Sun sensors and that the field-of-view (FOV) of the Sun sensors needs to be wide enough that there will be no gaps between sensors on different sides. Since the sensors are placed at a 90-degree angle to each other the minimum FOV of each sensor should be 90 degrees. To have some overlap between the sensors a FOV of 100 degrees is required.

Fine Sun sensors are desired to provide the required attitude info for accurate pointing of the satellite for the high-speed communication and earth observation payloads. For fine pointing accuracy the Sun sensors should have an accuracy of 0.1 degrees or better.

Sun sensors need to be able to function in direct sunlight without saturating or losing accuracy, to achieve this the exposure of the sensor needs to be low enough that direct sunlight entering the sensor does not saturate it or increase the measurement error significantly. The maximum peak intensity must not exceed 80% of the maximum sensor intensity.

Since the satellite will be spun up to one revolution per second the Sun sensor needs to work accurately enough to provide accurate readings even while the satellite is spinning [7]. To achieve the required accuracy the time of the measurement must be determined as accurately as possible. To achieve an accuracy of 1 degree the measurement time inaccuracy must be less than 4 ms.

4.3 Design overview

Each Sun sensor consists of two 1D image sensors that are placed perpendicularly to each other. The sensors are covered by a stainless-steel mask that has two narrow slits cut into it. The slits are perpendicular to the image sensors. Figure 2 shows an example of a digital Sun sensor.

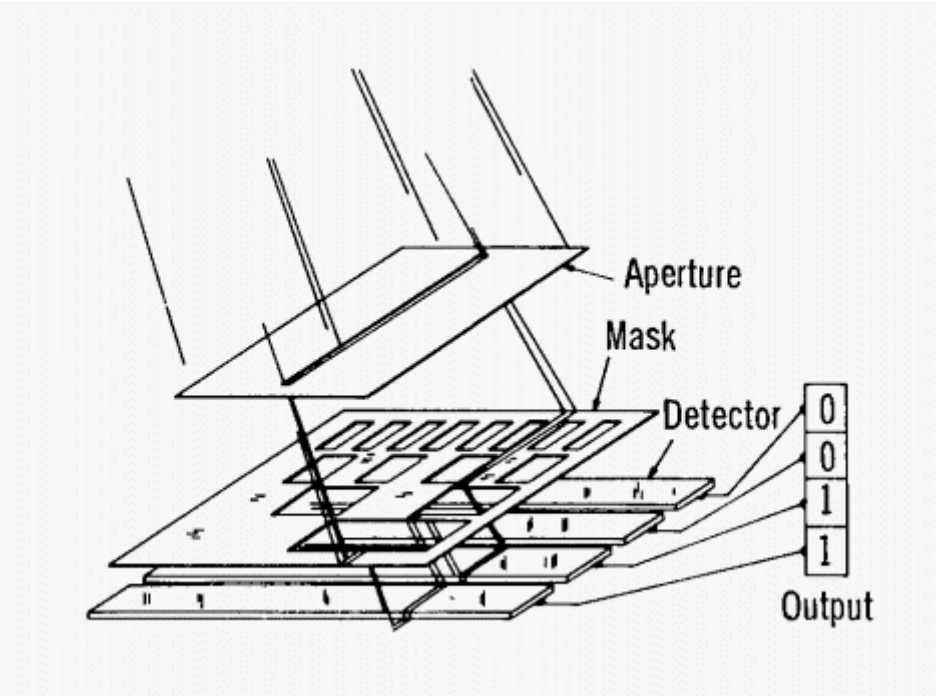

Figure 2: Example of a Sun sensor [18]

The mask blocks out most of the light and allows only a narrow beam to enter the sensor. The width of the light beam is determined by the width of the slit in the mask. By measuring what part of the sensor that beam hits we can calculate the angle of the satellite with respect to that light source. In space the main light source will be the Sun, so the angle will be with respect to the Sun.

The accuracy of the Sun sensor can be increased further by making the slit narrow enough that a diffraction pattern will form on the sensor. A function can then be fitted to that diffraction pattern, this will give the sensor sub-pixel accuracy. [19]

Linear image sensors were chosen as the basis for the Sun sensors because the data from the sensors can be filtered to give a more accurate reading. On ESTCube-1 Sun sensors based on a position sensitive device were used and there were problems with unwanted light sources, like Earth albedo, skewing the results [20]. Hopefully this can be avoided with a linear image sensor based design where unwanted light sources can be ignored more easily.

4.4 Hardware

Multiple sensors were considered but, in the end, s9226 sensors from Hamamatsu were chosen. These sensors were chosen for their pixel count, size and their small pin count. CMOS sensors were chosen because they capture an entire row of pixels at once, this allows more accurate measurements to be made. Each image sensor has 1024 pixels, that means that each Sun sensor measurement has 2048 values. [21]

The sensors are connected directly to the MCU, each sensor requires 5 MCU pins for operation. Each sensor requires a clock signal and a start signal to start measuring. During the measurement process the sensor will output each pixel in serial as an analog value. Along with each pixel the sensor will also output a trigger signal that can be used to determine when to read each pixel. The pixels are converted using the internal ADC on the MCU. At the end of the measurement an EOS signal is sent by the sensor that indicates that all the pixels have been sent. [21]

4.5 Software

Prototype software for the sensor is written to run on the side panel MCU, the current version of the software only saves the measured values to memory and sends them over UART. To achieve high accuracy at high spin rates the delay between a start signal and start of the measurement needs to be as small as possible to achieve precise timing of the measurements. The measurement speed must also be as fast as possible. To achieve this an algorithm was developed that has as little overhead as possible.

4.5.1 Measurement algorithm

A block diagram of the algorithm used to take a Sun sensor reading can be seen in Figure 3. First a clock signal is generated using timer compare match functionality. Both sensors have a common clock signal to keep them synchronized. This is achieved by connecting the clock pins of both sensors to the same MCU pin.

Then the program waits for a signal to start the measurement, this signal can for example be a start command sent to the MCU over UART or an internal signal sent after the last measurement is finished.

Once a start signal is received the program makes a dummy measurement to set the exposure of the real measurement. This is required because the speed of the real measurement is limited by the speed of the analog to digital converter (ADC) of the MCU. Since the data from the dummy measurement is not saved the sensor can be run at a higher clock speed than for the main measurement. The sensor can even be overclocked to lower the exposure even more.

After the dummy measurement is finished the clock frequency is set to the actual frequency used for measurements and a new start pulse is given. The program then enters a loop where it waits for a trigger signal from the sensor. Since both sensors are synchronized only one trigger signal is needed for both. Once the program receives the trigger signal an ADC conversion is started, the ADC converts pixels from both sensors automatically. After the conversion is finished the pixels are transferred to RAM using DMA.

When the sensors finish sending out pixels an EOS signal is generated, when the program receives this EOS signal it waits for the last transfer of pixels to finish and then starts a new measurement.

4.5.2 Algorithm performance

The developed algorithm works as designed and does not limit performance of the sensor, the main limit factor becomes the speed of the ADC that is only capable of 200 000 conversions a second, since the sensors are also capable of measuring at 200 ksps and there are two sensors the actual measurement rate is 100 ksps, which is half of the maximum possible output of the sensors.

The accuracy of the measurement start time depends on the overhead of the algorithm and can be compensated for if this overhead is consistent. Without any compensation the delay time between receiving a start signal and time of the actual measurement is approximately 0.2 ms, this gives the sensor a measurement accuracy of 0.072 degrees while spinning at 1 revolution per second.

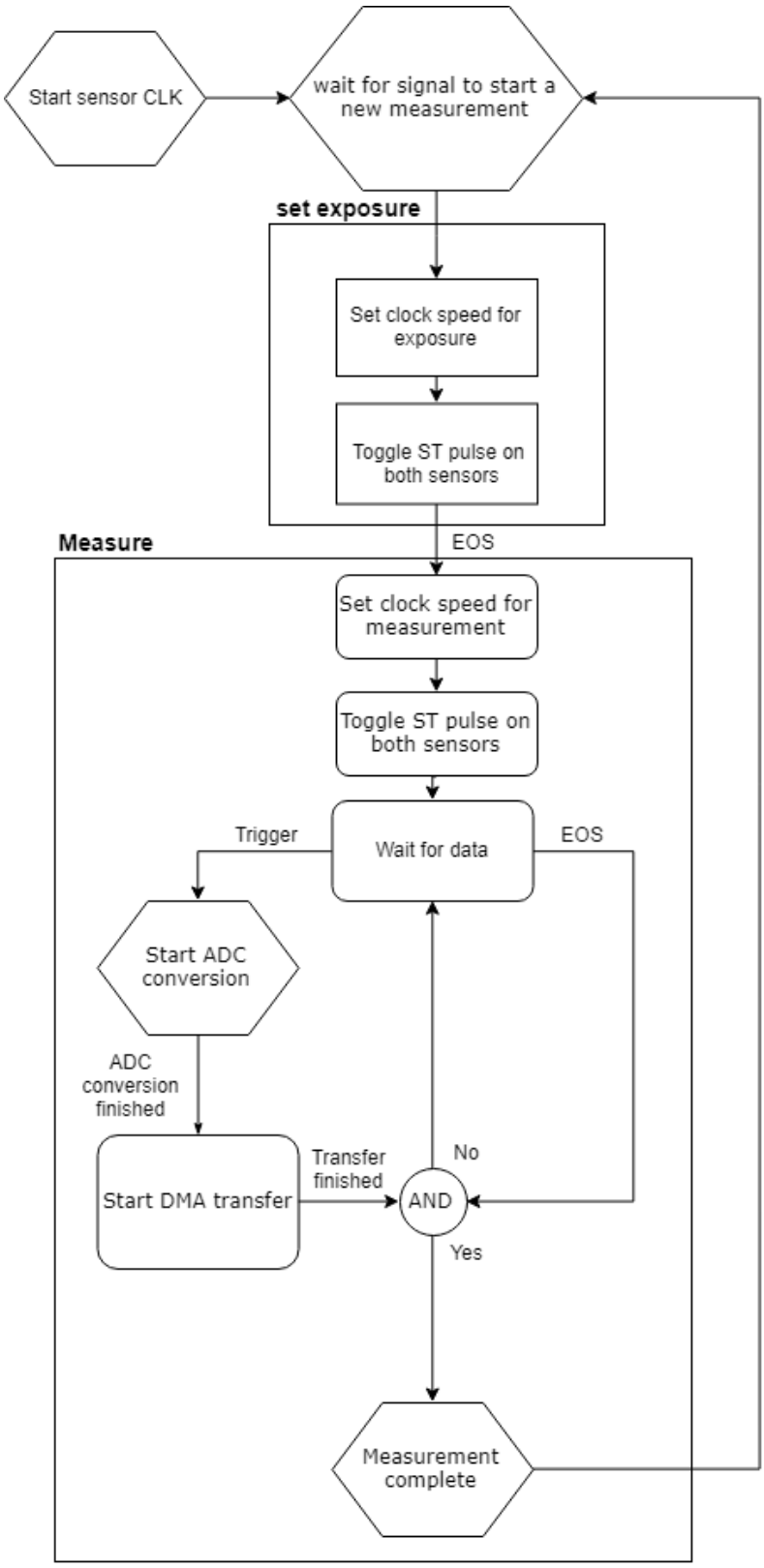

Figure 3: Block diagram of the Sun sensor algorithm

4.6 Testing and results

The prototype sensor was tested at the optics laboratory in Tartu Observatory. Two tests were carried out, a test with a point light source to determine the linearity and FOV of the sensor and a test with a Sun simulator to determine the performance of the sensor in sunlight.

4.6.1 Test setup

For the linearity and FOV tests the Sun sensor was set up in a dark room on a high precision rotating bench with a point light source pointed directly at the sensor. The sensor and the light source were aligned using a laser alignment tool, a picture of the test setup can be seen in Figure 4.

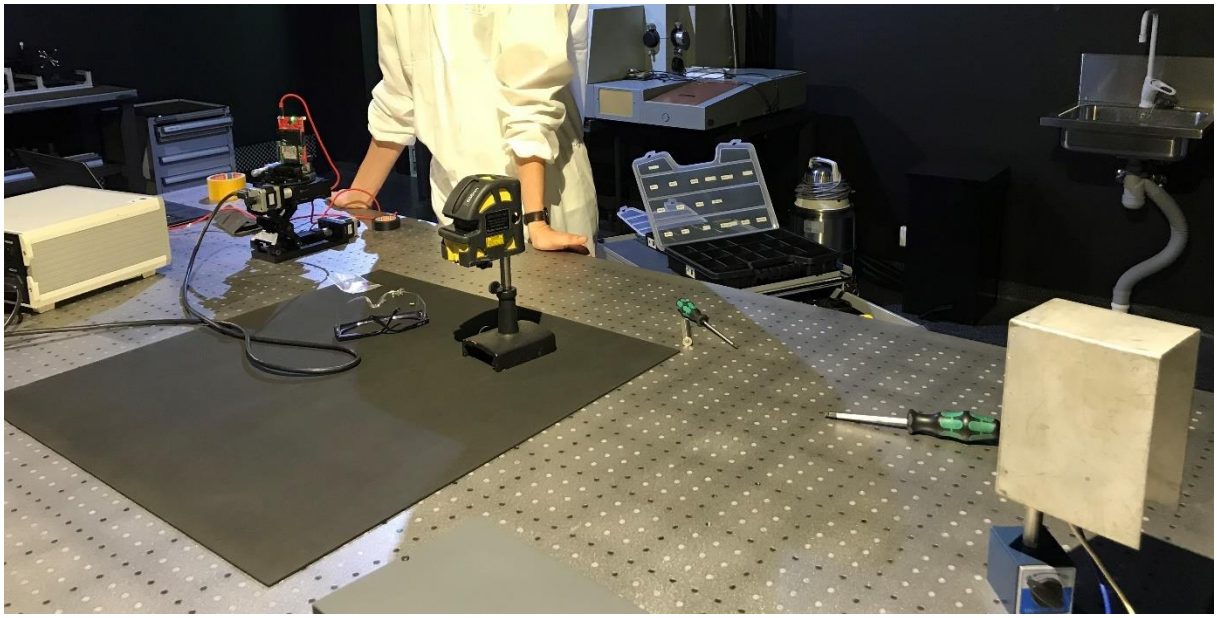

Figure 4: test setup for Sun sensor rotation tests

For the test with the Sun simulator the sensor was placed under the solar simulator and the simulator was turned on at 100% intensity. Picture of the test setup can be seen in Figure 5.

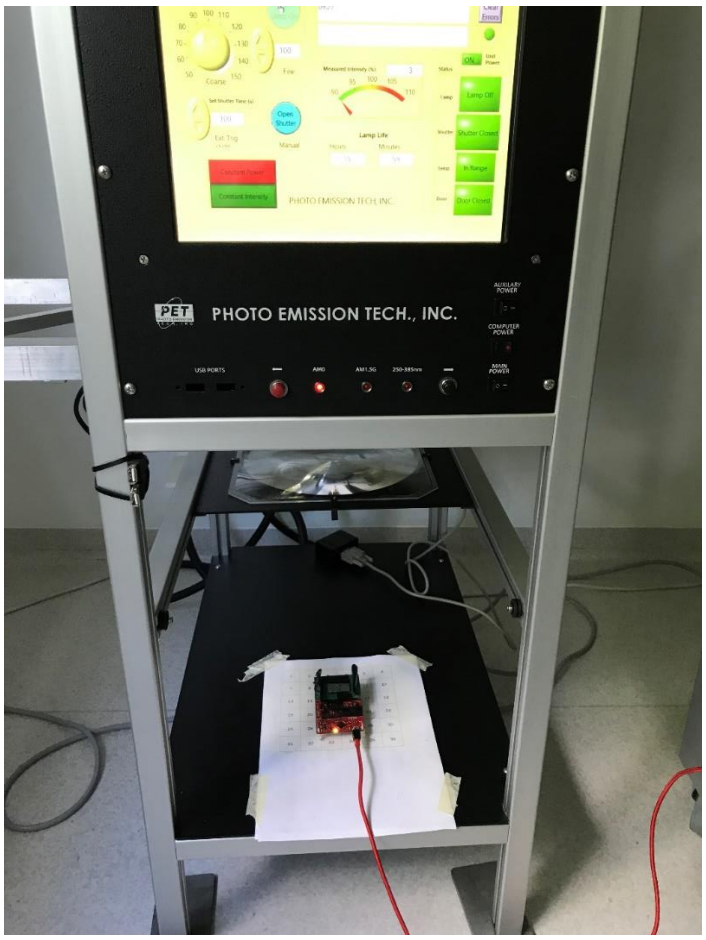

Figure 5: test setup for Sun sensor intensity tests

4.6.2 Testing procedure

For the rotation tests the rotation bench was first centered to the light using a mirror and a laser alignment tool and the center point was noted down. Then the sensor was rotated in one direction until a peak could no longer be seen in the output of the sensor, meaning that the light was outside the FOV of the sensor. The sensor was then rotated in steps of 2 degrees in the other direction until the peak could no longer be seen. Location and size of the peak was measured at every step.

For the intensity tests the Sun sensor was placed under the Sun simulator and an initial value was recorded with the simulator off, then the simulator was turned on and the value of the sensor was recorded again. This test was repeated with different filters in front of the sensor to determine a specific filter in front of the sensor that could help with the saturation of the sensor.

4.6.3 Test results

The data collected from the rotation bench tests was processed to remove noise from the data. The clean data was then used to calculate the FOV and the linearity of the sensor.

To calculate the FOV the intensity of the sensor was plotted over the angle of the sensor from the center point. From the resulting graph the angles at which the intensity became equal to the noise floor were found. The FOV of the sensor was calculated by subtracting the two angles where the cut-off happened. The FOV of the sensor was found to be 68 degrees which does not meet the requirements.

The reason for the small FOV can be seen by looking at a graph of peak intensity at different positions on the sensor, as shown in Figure 6. The graph shows us that the intensity of the peaks reduces as we get closer to the edge of the sensor and becomes indistinguishable from the sensor noise floor at around 250 and 750 pixels. This sudden drop off in intensity is most likely caused by the mask blocking the light beam from reaching the edges of the sensor which means the slit of the mask needs to be higher. The slit could also be made wider to increase the FOV.

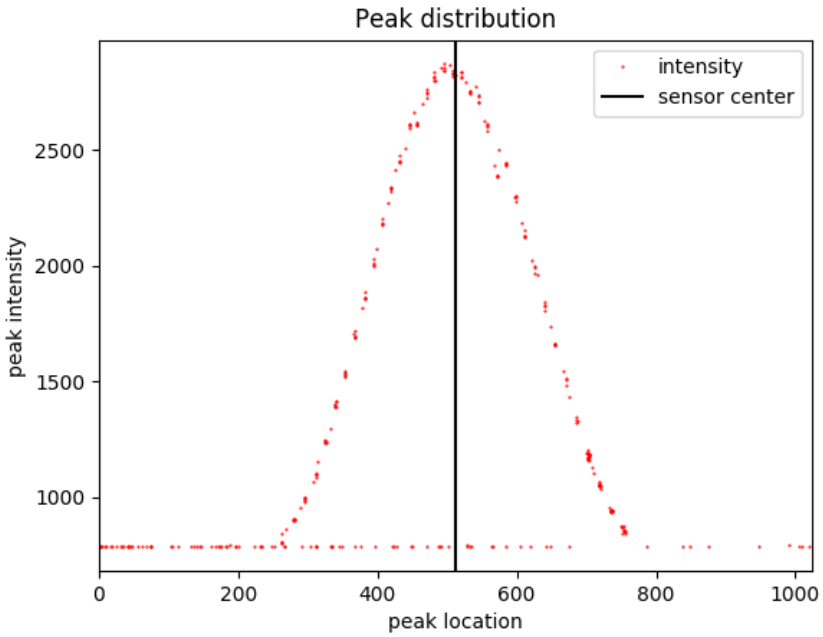

Figure 6: Intensity of peaks over the sensor

Linearity of the sensor over the FOV was also determined, this was done by fitting a linear function to the actual angles and measured peak locations, this function was then used to estimate the angle from the peak locations. The results can be seen in Figure 7. The sensor is linear in the entire FOV with a standard deviation of 0.65 degrees from the actual angle.

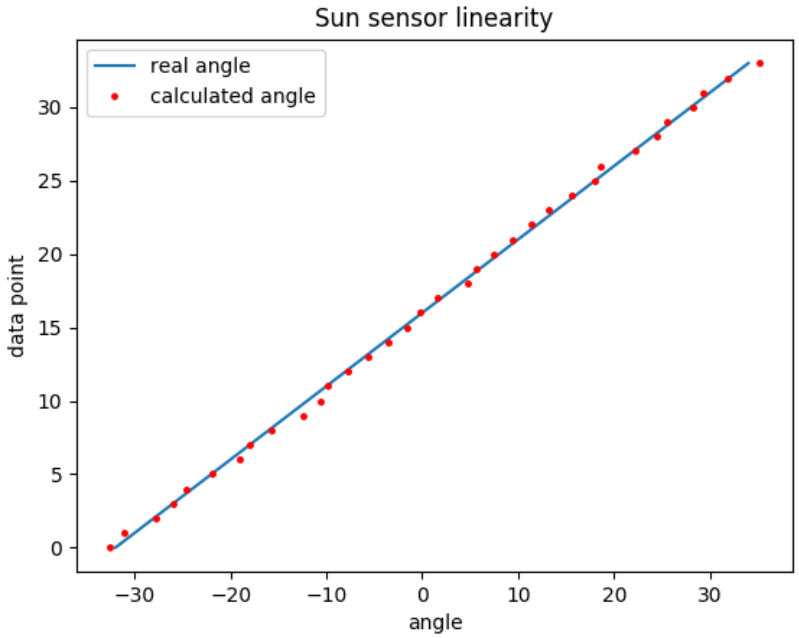

Figure 7: Sun sensor linearity

Data from the intensity tests with a Sun simulator showed that without a filter in front of the mask the sensor saturates so much in direct Sun light that it stops outputting data. Several filters were tested to see if some of the light could be blocked off so that the sensor no longer saturates in direct sunlight. The filter that gave the best results was UFS-1, the filter permittivity at different wavelengths can be seen in Figure 8. The filter blocks out most of the light in the wavelengths where sunlight has the highest intensity. By analyzing the information provided by this test it is possible to choose the correct filter for the next prototype of the Sun sensor.

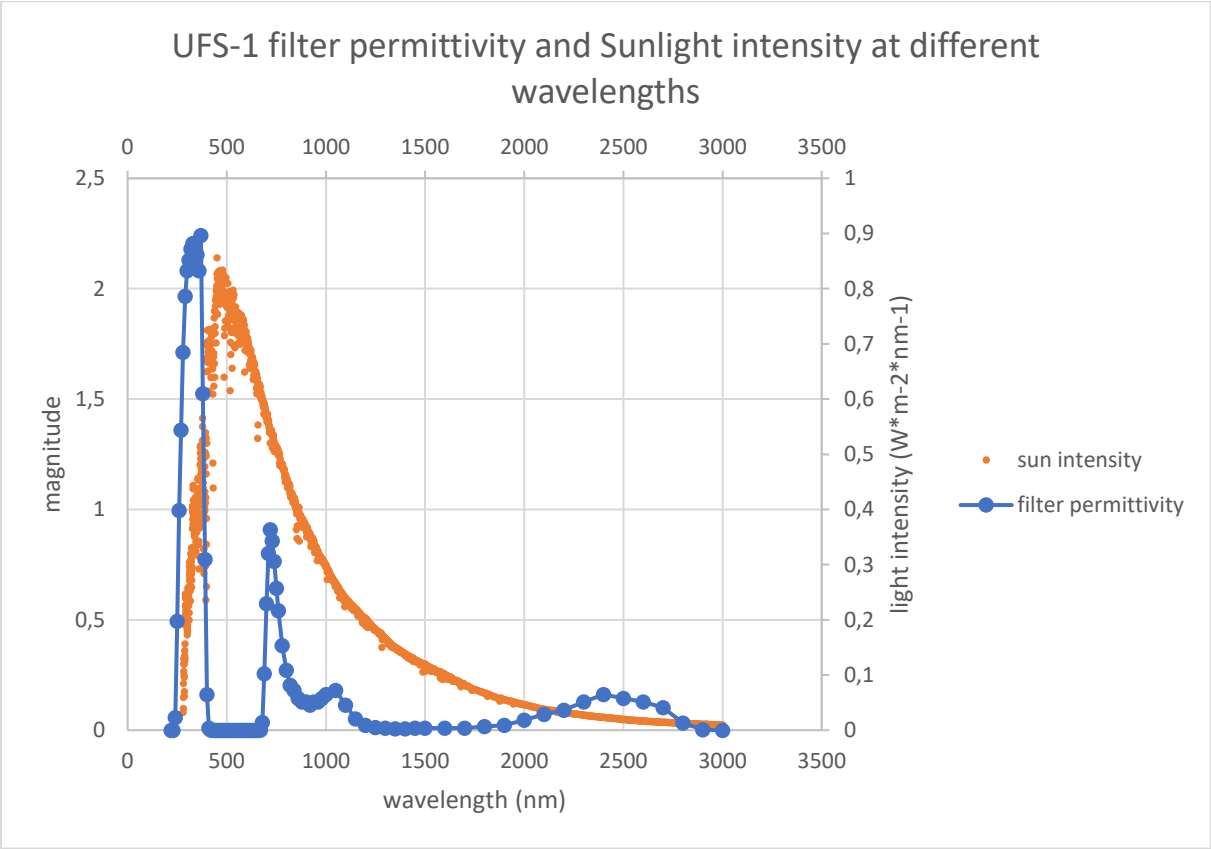

Figure 8: UFS-1 filter permittivity and sunlight intensity at different wavelengths [22]

5 Magnetorquers

Magnetorquers are electromagnets that can be used to control the satellites attitude, they work by generating a magnetic field that interacts with Earth's magnetic field to create a torque. This torque tries to align the satellites magnetic field with Earth's magnetic field, making the satellite rotate.

The satellite will have a total of three magnetic coils, one on every axis of the satellite. This allows the satellite to freely change its attitude in all directions. Only two of the coils are on the side panels, the third one is part of the main satellite bus.

The coils are connected to a coil driving circuit that allows the MCU to control the direction and size of the current going through the coils. This is needed to control the torque generated by the coils and control the satellites attitude accurately.

5.1 Overview of other magnetorquers

Magnetic torque is one of the most popular methods for nanosatellite attitude control, with around 65% of nanosatellites having some form of magnetorquers on board [13].

Magnetorquers can be divided into two distinct groups, active and passive magnetorquers. Passive magnetorquers are just permanent magnets that passively align the satellite with Earths' magnetic field. Active magnetorquers, like the ones used on ESTCube-2 use controllable electromagnets to actively control the attitude of the satellite.

Active magnetorquers can be divided into two groups, air-core magnetorquers also known as coils and ferromagnetic core magnetorquers also known as rods. The main differences between the two is the shape of the torquer and the size of the magnetic moment produced. Air coils usually provide a lower magnetic moment but can be made more compact since the center is empty. Rods provide a higher magnetic moment but may have a residual magnetic moment after being turned off since the core still retains its magnetism. [23]

Many COTS magnetic torquer modules are available, but these are usually very costly and have a fixed size that needs to be worked around. [24] [25]

ESTCube-2 will use air coils since air coils have a more flexible size compared to rods, this allows us to fit the coils inside the side panels where space is limited. The coils are manufactured in-house using the same tools that were used for ESTCube-1 magnetic coils that have been proven to work in space. [26]

5.2 Magnetorquer coils

ESTCube-2 magnetorquers are based on the magnetorquers used on ESTCube-1, the size of the coils has been increased to give ESTCube-2 higher magnetic torque. The coils are built in house using a coil winding robot developed for ESTCube-1 [27].

5.2.1 Coil requirements

ESTCube-1 had coils with a magnetic moment of 0.1 Am^2, in-flight measurements showed that the satellite had a large residual magnetic moment which was of almost the same strength as the electromagnetic coils [26]. Based on these results it was decided that ESTCube-2 coils should have at least double the magnetic moment of the ESTCube-1 coils, to overcome the residual magnetic moment of the satellite. The coils should have a magnetic moment of at least 0.2 Am^2.

The physical size of the coils is determined by the space available inside the side panels of the satellite. To maximize the available magnetic torque two different sized coils have to be made. The coil on the Z axis has a maximum size of 80 mm by 80 mm and the coils on the X and Y axis have a maximum size of 120 mm by 60 mm.

5.2.2 Coil design

Multiple coil shapes were considered, originally the coils had an internal area of a square with rounded corners, but after making prototype coils it was determined that this design is not suitable because the corners of the coil do not adhere to the mold properly. The coils were redesigned to be more circular.

Based on the requirements two coil designs were made, one for Z axis and one for the X and Y axis. The coil on the Z axis will be a circle with a diameter of 80 mm. A prototype Z axis coil

can be seen in Figure 9. The coils on the X and Y axis will be oval with a width of 120 mm and a height of 60 mm.

Figure 9: Prototype Z axis coil

The magnetic moment of N number of loops with equal areas can be calculated using Equation 1 where m is the magnetic moment, N is the number of loops, I is the current in the coil and S is the area of the coil.

$$\boldsymbol{m} = NI\boldsymbol{S}$$

Equation 1

The actual coils will have multiple layers, so to get the magnetic moment of the whole coil the magnetic moments of all the layers must be added. To make the calculations a Python script was created, that calculated the resistance, current, power and magnetic moment of the coils based on the inputs. The inputs and results of these calculations can be seen in Table 2. The inputs are marked with a green background and the outputs are marked with a yellow background.

Table 2: Coil parameters

attribute	X and Y coils	Z coil
Width	120	80 mm
Height	60	80 mm
thickness	2.5 mm	4 mm
Wire thickness	0.18 mm	0.26 mm
Number of turns	400	400
Voltage	10 V	10 V
Length	113.9 m	96.3 m
Current	133 mA	328.2 mA
Resistance	75.2 Ω	30.47 Ω
Power	1.33 W	3.28 W
Magnetic moment	0.27 Am^2	0.58 Am^2

The calculations show that both coils will have sufficient magnetic moment to meet the design requirements.

5.3 Coil driver

Two different prototypes were designed for the coil driver circuit. This was done because during testing it was determined that the original design is not capable of the required performance.

5.3.1 Design requirements

The main requirement of the coil driver circuit is that it needs to be able to provide the required current and voltage to the coils to achieve the desired magnetic moment. This means that the coil driver should be able to provide a current of 330 mA at 10 V to the coils.

The coil driver also needs to control the direction and magnitude of the current accurately so that the satellites attitude can be controlled accurately. The coil current must be linearly controllable in the full range from 0 mA up to the maximum current needed. To achieve the required control accuracy the magnetic moment needs to be controllable in at least 1% increments, the coil driver must be able to provide sufficiently fine current control to achieve this.

5.3.2 First prototype

The first design was based on a LED driver IC, that had a built in constant current boost regulator. The output current of the LED driver was controllable using PWM. The circuit included an external H-bridge to control the direction of the current through the coil.

The chosen driver was TPS61165 from Texas Instruments, the driver was chosen because it met the design requirements for output current and voltage. [28]

During testing it was determined that the LED driver was only controllable at PWM duty cycles of around 40% and above, this would have given us only 60% of the maximum current range, which does not meet the design requirements. Figure 10 shows the output current of the driver at different PWM duty cycles and at different voltages. It can be clearly seen that by increasing the voltage the usable range of PWM duty cycles decreases.

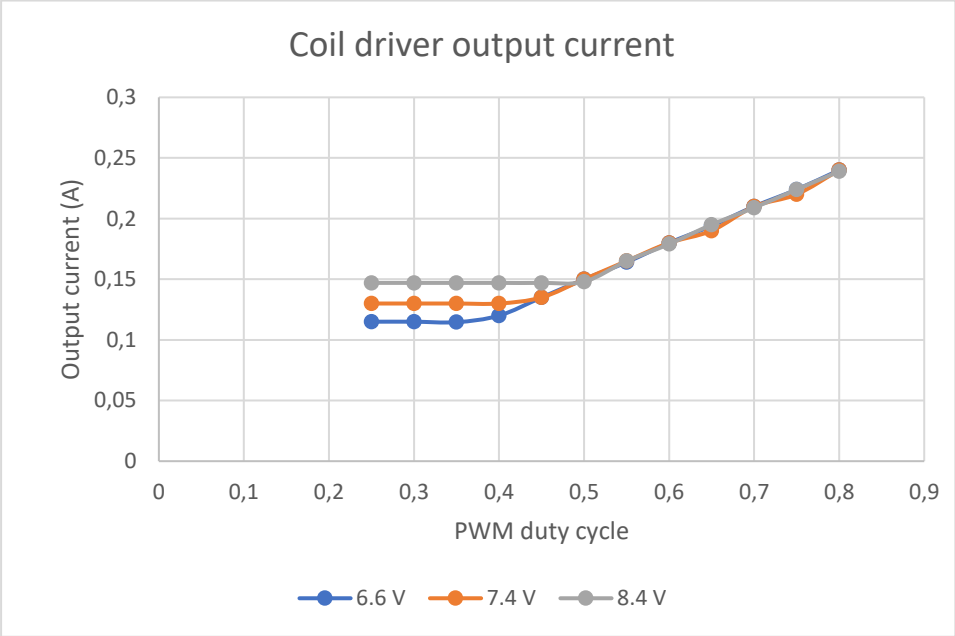

Figure 10: Coil driver output current in relation to PWM duty cycle

Testing also showed that the LED driver was less efficient at lower voltages, this can be seen in Figure 11 where efficiency at different voltages and PWM duty cycles is shown. It can be clearly seen that by increasing the voltage efficiency also increases.

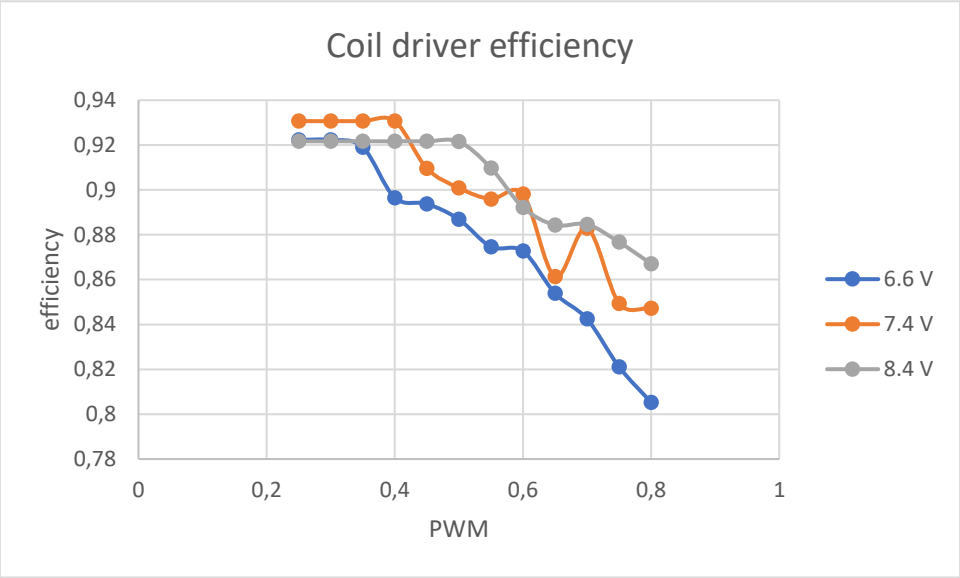

Figure 11: Coil driver efficiency at different voltages and PWM duty cycles

5.3.3 Final design

After testing of the first design it was decided to redesign the coil driver circuit completely. The new design is based on the coil driver used on ESTCube-1, this approach was chosen because it has been shown to work for similar coils to the ones that will be used on ESTCube-2. [20] A block diagram of the design can be seen in Figure 12.

The new circuit is based on the DRV8837 motor controller from Texas Instruments. This controller was chosen because it meets the design requirements for maximum current and voltage. Since the driver has an integrated H-bridge, the external H-bridge was removed from the circuit. [29]

A boost converter is used to boost the voltage into the motor controller, this was required because the voltage provided by the satellite bus is unregulated and can drop too low to provide sufficient current to the coils. The chosen boost converter is LMR62014 from Texas Instruments. The boost converter can be bypassed if the voltage from the satellite bus is high enough that it is not required. [30]

A low pass RC filter is placed between the output of the motor driver and the coil to turn the PWM signal output from the motor driver into constant voltage for the coil. A simple RC filter was chosen to simplify the design and avoid unnecessary components. The PWM signal is not suitable for driving the coil because the changing voltage would create a reactance in the coil that is undesired for a magnetorquer.

The new design also includes a current measurement circuit, that is need for the MCU to be able to measure the current on the coil. This circuit is based on the INA199 current measurement IC. The current measurement IC is connected in parallel to a shunt resistor right before the motor driver. This location was chosen because the current at that location only flows in one direction, after the motor driver the current could flow in two directions which would require a more complicated design to measure. By measuring the current before the motor driver, the efficiency of the motor driver must be considered, as some of the current will be lost as heat. [29]

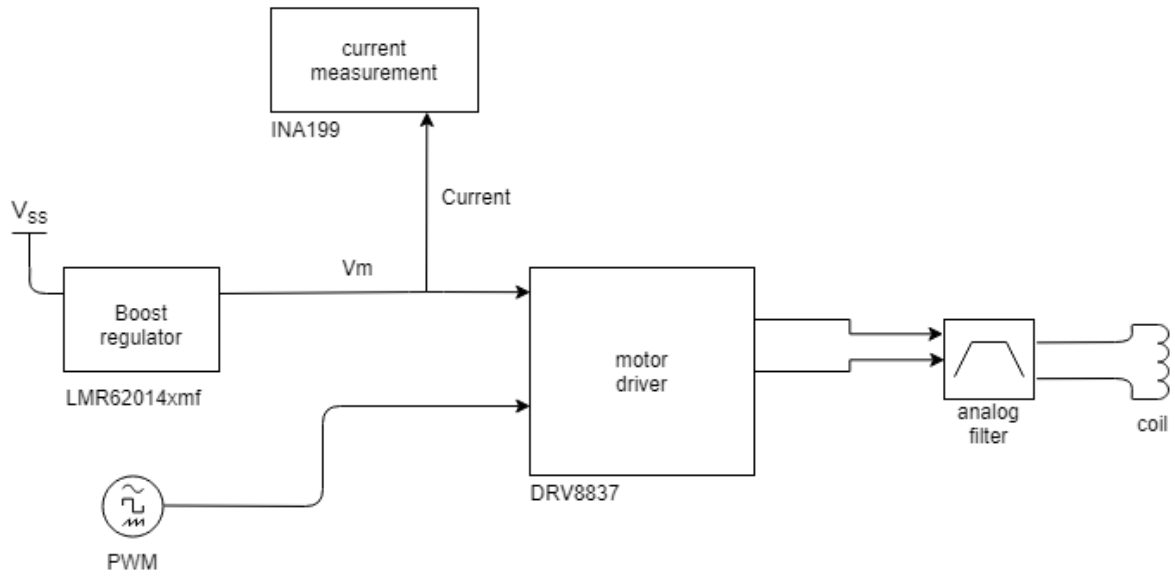

Figure 12: Coil driver block diagram

5.4 Magnetorquer testing

5.4.1 Test setup

Magnetorquers are tested in two parts, first the coil driver and the coils are tested in a lab to verify that they meet their design requirements. The coil driver must be able to output the required current and voltage and the coil must have the required resistance. The coil driver is tested by connecting it to a laboratory power supply and a signal generator, a load is connected to the output of the coil driver and an oscilloscope is used to measure the waveform at the output.

When the coil driver and the coil have been both verified to meet the design requirements separately then they are tested together to determine the magnetic moment generated by the coil. To measure the magnetic moment of the coil it is placed in a Helmholtz coil at Tartu Observatory where the magnetic torque can be measured.

5.4.2 Test results

A prototype coil has been tested in the laboratory, resistance and inductance of the coil were measured at different frequencies. Calculated parameters of the tested coil can be seen in Table 3. The measured values are shown in Figure 13. At low frequencies the measured coil resistance is similar to the calculated resistance, but at higher frequencies the resistance rises significantly.

Table 3: Calculated prototype coil parameters

parameter	value
Radius	40 mm
Thickness	4 mm
Wire thickness	0.18 mm
Resistance	69.9 Ω
Magnetic moment	0.21 Am^2

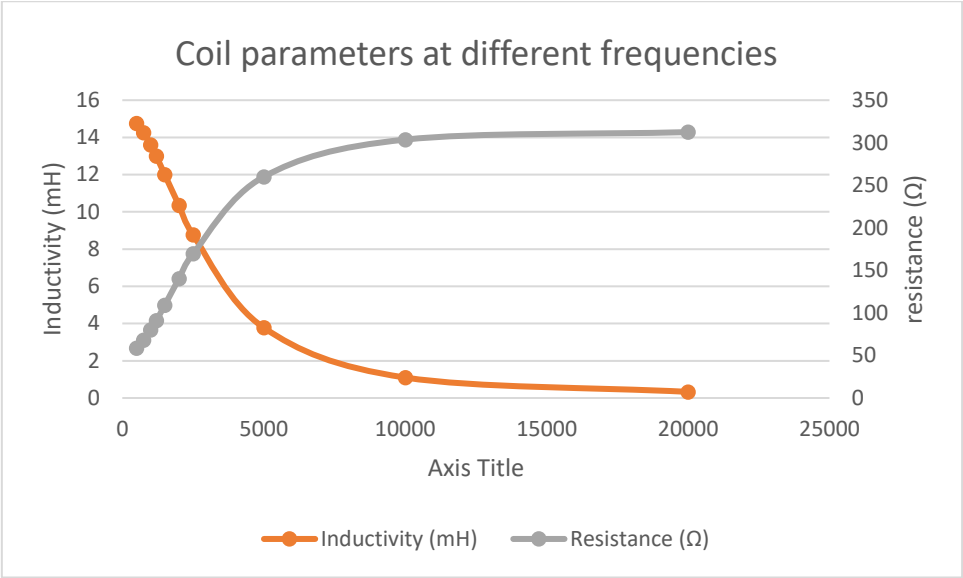

Figure 13: Measured prototype coil parameters

The testing of the final coil driver design is still ongoing at the time of writing of this thesis, so the results cannot be published here.

6 Conclusions and future work

During this thesis two modules for the side panels were developed and tested, sun sensors and magnetorquers.

Software for a prototype sun sensor was developed and initial tests of the sun sensor were carried out. The results of these tests show that the prototype sun sensor has a field of view of 68 degrees and a standard deviation of 0.65 degrees over the whole FOV. Testing also showed that the sensor saturates when placed in direct sunlight and that by placing a filter in front of the sensor that saturation can be avoided.

In the future in-depth filter testing must be carried out and the sensor design must be altered to accommodate the filter in front of the sensor and to increase the FOV of the sensor.

A prototype coil driver and magnetic coils were designed and developed based on the set requirements. Preliminary testing of the coils was completed that showed that the parameters of the prototype coils are similar to the calculated parameters. Testing of the coil driver electronics was started but was not completed in time for the publication of the thesis.

The testing of coil driver electronics needs to be completed, then the coil driver and the coils can be tested together in a Helmholtz coil to determine if the calculated magnetic moment matches the real magnetic moment produced by the coils.

Once the modules have been tested a prototype side panel can be designed and manufactured. This prototype will then be used to test the side panels with the OBC of the satellite.

Acknowledgments

The author would like to thank his supervisors Hendrik Ehrpais and Erik Ilbis for their advice and guidance during the writing of the thesis, their help was invaluable in completing this thesis.

Additionally, the author would like to thank all the members of the ESTCube team for providing me with the opportunity to work on this awesome project.

Finally, the author would like to thank his family for moral support during the thesis writing process

Aleksander Parelo

References

[1] The CubeSat Program, Cal Poly SLO, "CubeSat," 20 2 2014. [Online]. Available: https://static1.squarespace.com/static/5418c831e4b0fa4ecac1bacd/t/56e9b62337013b6c063a655a/1458157095454/cds_rev13_final2.pdf. [Accessed 1 04 2018].

[2] S. . Lätt, A. . Slavinskis, E. . Ilbis, U. . Kvell, K. . Voormansik, E. . Kulu, M. . Pajusalu, H. . Kuuste, I. . Sünter, T. . Eenmäe, K. . Laizans, K. . Zalite, R. . Vendt, J. . Piepenbrock, I. . Ansko, A. . Leitu, A. . Vahter, A. . Agu, E. . Eilonen, E. . Soolo, H. . Ehrpais, H. . Lillmaa, I. . Mahhonin, J. . Mõttus, J. . Viru, J. . Kalde, J. . Šubitidze, J. . Mucenieks, J. . Šate, J. . Kütt, J. . Poļevskis, J. . Laks, K. . Kivistik, K.-L. . Kusmin, K.-G. . Kruus, K. . Tarbe, K. . Tuude, K. . Kalniņa, L. . Joost, M. . Lõoke, M. . Järve, M. . Vellak, M. . Neerot, M. . Valgur, M. . Pelakauskas, M. . Averin, M. . Mikkor, M. . Veske, O. . Scheler, P. . Liias, P. . Laes, R. . Rantsus, R. . Soosaar, R. . Reinumägi, R. . Valner, S. . Kurvits, S.-E. . Mändmaa, T. . Ilves, T. . Peet, T. . Ani, T. . Tilk, T. C. Tamm, T. . Scheffler, T. . Vahter, T. . Uiboupin, V. . Evard, A. . Sisask, L. . Kimmel, O. . Krömer, R. . Rosta, P. . Janhunen, J. . Envall, P. . Toivanen, T. . Rauhala, H. . Seppänen, J. . Ukkonen, E. . Hæggström, R. . Kurppa, T. . Kalvas, O. . Tarvainen, J. . Kauppinen, A. . Nuottajärvi, H. . Koivisto, S. . Kiprich, A. N. Obraztsov, V. . Allik, A. . Reinart and M. . Noorma, "ESTCube-1 nanosatellite for electric solar wind sail in-orbit technology demonstration," , 2014. [Online]. Available: http://elib.dlr.de/104899. [Accessed 16 5 2018].

[3] S. . Busch, P. . Bangert, S. . Dombrovski and K. . Schilling, "UWE-3, in-orbit performance and lessons learned of a modular and flexible satellite bus for future pico-satellite formations☆," *Acta Astronautica,* vol. 117, no. , pp. 73-89, 2015.

[4] S. Speretta, L. M. Reyneri, C. Sansoe, M. Tranchero, C. Passerone and D. D. Corso, "Modular architecture for satellites," in *58th International Astronautical Congress*, Hyderabad, 2007.

[5] E. . Ilbis, "System Architecture and Component Evaluation for ESTCube-2 Electrical Power System," , 2016. [Online]. Available: http://dspace.ut.ee/handle/10062/51869. [Accessed 16 5 2018].

[6] ISIS space, "ISIS Space," 22 September 2014. [Online]. Available: https://www.isispace.nl/wp-content/uploads/2015/12/ISIS.STS_.0.1.003-RevB-Sheet1-1-3U-CubeSat-Dimensions-A0.pdf. [Accessed 16 May 2018].

[7] I. Iakubivsky, H. Ehrpais, J. Dalbins, E. Oro, E. Kulu, J. Kütt, P. Jahunen, A. Slavinskis, E. Ilbis, I. Ploom, I. Sünter, R. Trops and M. Merisalu, "ESTCube-2 mission analysis: plasma brake experiment for deorbiting," in *67th International Astronautical Congress (IAC)*, Guadalajara, Mexico, 2016.

[8] S. . Busch and K. . Schilling, "Robust and Efficient OBDH Core Module for the Flexible Picosatellite Bus UWE-3," *Automatic control in aerospace,* vol. 46, no. 19, pp. 218-223, 2013.

[9] M. Põder, "Prototype Design of ESTCube-2 Electrical Power System Control Electronics," 2015.

[10] S. Tammesoo, "Suhtlusprotokoll ESTCube-2 alamsüsteemide vaheliseks suhtluseks," 2015.

[11] Linear Technologies, "LTC2850/LTC2851/LTC2852 3.3V 20Mbps RS485/RS422 Transceivers," Linear Technology Corporation, Milpitas, 2007.

[12] M. K. Nigol, "ESTCube-2 attitude and orbit control system sensor selection and temperature calibration," 2017.

[13] J. . Bouwmeester and J. . Guo, "Survey of worldwide pico- and nanosatellite missions, distributions and subsystem technology ☆," *Acta Astronautica,* vol. 67, no. , pp. 854-862, 2010.

[14] Maryland Aerospace, Inc, "MAI Sun sensor," Maryland Aerospace, Inc, Crofton, 2015.

[15] Solar MEMS Technologies S.L., "nanoSSOC-D60," Solar MEMS Technologies S.L., Sevilla, 2016.

[16] M. . Taraba, C. . Rayburn, A. . Tsuda and C. . MacGillivray, "Boeing's CubeSat TestBed 1 Attitude Determination Design and On-Orbit Experience," , 2009. [Online]. Available: http://digitalcommons.usu.edu/cgi/viewcontent.cgi?article=1325&context=smallsat. [Accessed 20 5 2018].

[17] P. M. Rodrigues and P. M. Ramos, "Design and characterization of a sun sensor for the SSETI-ESEO project," in *XVIII IMEKO WORLD CONGRESS Metrology for a Sustainable Development*, Rio De Janeiro, 2006.

[18] NASA, "Spacecraft sun sensors," NASA, Washington D.C., 1970.

[19] H. . Ehrpais, "ESTCube-2 attitude and orbit control system design," , 2017. [Online]. Available: http://dspace.ut.ee/handle/10062/56543. [Accessed 16 5 2018].

[20] A. Slavinskis, E. Kulu, J. Viru, R. Valner, H. Ehrpais, T. Uiboupin, M. Järve, E. Soolo, J. Envall, T. Scheffler, I. Sünter, H. Kuuste, U. Kvell, J. Kalde, K. Laizans, E. Ilbis, T. Eenmäe, R. Vendt, K. Voormansik, I. Ansko, V. Allik, S. Lätt and M. Noorma, "Attitude determination and control for centrifugal tether deployment on the ESTCube-1 nanosatellite," vol. 2S, no. 63, 2014.

[21] Hamamatsu, "CMOS linear image sensors S9226 series," 2017.

[22] "Reference Solar Spectral Irradiance: Air Mass 1.5," , . [Online]. Available: http://rredc.nrel.gov/solar/spectra/am1.5/. [Accessed 18 5 2018].

[23] F. . Mesch, "Magnetic components for the attitude control of space vehicles," *IEEE Transactions on Magnetics,* vol. 5, no. 3, pp. 586-592, 1969.

[24] ISIS - Innovative Solutions In Space B.V., "Magnetorquer Board (iMTQ)," ISIS - Innovative Solutions In Space B.V., Delft.

[25] CubeSatShop, "CubeSatShop," [Online]. Available: https://www.cubesatshop.com/product/mt01-compact-magnetorquer/. [Accessed 20 May 2018].

[26] H. . Ehrpais, J. . Kütt, I. . Sünter, E. . Kulu, A. . Slavinskis and M. . Noorma, "Nanosatellite spin-up using magnetic actuators: ESTCube-1 flight results," *Acta Astronautica,* vol. 128, no. , pp. 210-216, 2016.

[27] T. Uiboupin, "ESTCube-1 elektromagnettõukurite automatiseeritud kerimisseadme arendus ja testimine," 30 May 2012.

[28] Texas Instruments, "TPS61165 datasheet," Texas Instruments, 2011.

[29] Texas Instruments, "DRV8837 datasheet," Texas Instruments, 2016.

[30] Texas Instruments, "LMR62014 SIMPLE SWITCHER® 20Vout, 1.4A Step-Up Voltage Regulator in SOT-23," Texas Instruments, 2013.

Appendix A – Side panel pin map

PINS										OVERVIEW				PINOUT PER SIDE											
pin	pin name	function	INT	DMA	ADC	COMP	SPI	UART	TIMER	all except Z-		Z-		X+		X-		Y+		Y-		Z+		Z-	
1	P1.0	ADC0	x	x	x	x			TA0-1	CLK	sun 1			CLK	sun 1	CLK	sun 1	CLK	sun 1	CLK	sun 1	CLK	sun 1	CLK	sun 1
2	P1.1	GPIO	x		x	x			TA0-2	CLK	sun 2			CLK	sun 2	CLK	sun 2	CLK	sun 2	CLK	sun 2	CLK	sun 2	CLK	sun 2
3	P1.2	GPIO	x		x	x			TA1-1	video	sun 1			video	sun 1	video	sun 1	video	sun 1	video	sun 1	video	sun 1	video	sun 1
4	P3.0	GPIO	x		x	x				trigger	sun 1			trigger	sun 1	trigger	sun 1	trigger	sun 1	trigger	sun 1	trigger	sun 1	trigger	sun 1
5	P3.1	GPIO	x		x	x				EOS	sun 1			EOS	sun 1	EOS	sun 1	EOS	sun 1	EOS	sun 1	EOS	sun 1	EOS	sun 1
6	P3.2	ADC14	x		x	x				solar_voltage	MPPT 2	video	sun 4									solar_voltage	MPPT 2	video	sun 4
7	P3.3	GPIO	x		x	x				bat_current	MPPT 2	EOS	sun 4									bat_current	MPPT 2	EOS	sun 4
8	P4.7	GPIO	x							EOS	sun 2			EOS	sun 2	EOS	sun 2	EOS	sun 2	EOS	sun 2	EOS	sun 2	EOS	sun 2
9	P1.3	GPIO	x		x	x	x		TA1-2	solar_current	MPPT 2	CLK	sun 4									solar_current	MPPT 2	CLK	sun 4
10	P1.4	ADC4	x		x	x	x		TB0-1	bat_voltage	MPPT 2	trigger	sun 4									bat_voltage	MPPT 2	trigger	sun 4
11	P1.5	ADC5	x		x	x	x		TB0-2	video	sun 2			video	sun 2	video	sun 2	video	sun 2	video	sun 2	video	sun 2	video	sun 2
12	PJ.0	GPIO				x				burning electronics				burning electronics								burning electronics		burning electronics	
13	PJ.1	GPIO				x				direction	magnettorquer					direction	magnettorquer	direction	magnettorquer						
14	PJ.2	GPIO				x				Start	sun 2			Start	sun 2	Start	sun 2	Start	sun 2	Start	sun 2	Start	sun 2	Start	sun 2
15	PJ.3	GPIO				x				Start	sun 1			Start	sun 1	Start	sun 1	Start	sun 1	Start	sun 1	Start	sun 1	Start	sun 1
16	P4.0	ADC8	x		x					bat_voltage	MPPT	Start	sun 3	bat_voltage	MPPT	bat_voltage	MPPT	bat_voltage	MPPT	bat_voltage	MPPT	bat_voltage	MPPT	Start	sun 3
17	P4.1	ADC9	x		x					bat_current	MPPT	video	sun 3	bat_current	MPPT	bat_current	MPPT	bat_current	MPPT	bat_current	MPPT	bat_current	MPPT	video	sun 3
18	P4.2	ADC10	x		x					solar_voltage	MPPT	trigger	sun 3	solar_voltage	MPPT	solar_voltage	MPPT	solar_voltage	MPPT	solar_voltage	MPPT	solar_voltage	MPPT	trigger	sun 3
19	P4.3	ADC11	x		x					solar_current	MPPT	EOS	sun 3	solar_current	MPPT	solar_current	MPPT	solar_current	MPPT	solar_current	MPPT	solar_current	MPPT	EOS	sun 3
20	P2.5	UART TX	x				x	TX A1	TB0-0	UART TX	ICP			UART TX	ICP	UART TX	ICP	UART TX	ICP	UART TX	ICP	UART TX	ICP	UART TX	ICP
21	P2.6	UART RX	x				x	RX A1	TB0-1	UART RX	ICP			UART RX	ICP	UART RX	ICP	UART RX	ICP	UART RX	ICP	UART RX	ICP	UART RX	ICP
22	TEST	I																							
23	RST	I/O																							
24	P2.0	GPIO	x				x	TX A0	TB0-6	UART TX	CAPCOR			UART TX	CAPCOR										
25	P2.1	GPIO	x				x	RX A0	TB0-0	UART RX	CAPCOR			UART RX	CAPCOR										
26	P2.2	UCB0CLK	x				x		TB0-2	SCLK	magnetometer			SCLK	magnetometer	SCLK	magnetometer	SCLK	magnetometer	SCLK	magnetometer	SCLK	magnetometer	SCLK	magnetometer
27	P3.4	GPIO	x						TB0-3	PWM	magnettorquer					PWM	magnettorquer	PWM	magnettorquer						
28	P3.5	GPIO	x						TB0-4	access_state	ICP			access_state	ICP	access_state	ICP	access_state	ICP	access_state	ICP	access_state	ICP	access_state	ICP
29	P3.6	GPIO	x						TB0-5	access_en	ICP			access_en	ICP	access_en	ICP	access_en	ICP	access_en	ICP	access_en	ICP	access_en	ICP
30	P3.7	GPIO	x						TB0-6	shutup_state	ICP			shutup_state	ICP	shutup_state	ICP	shutup_state	ICP	shutup_state	ICP	shutup_state	ICP	shutup_state	ICP
31	P1.6	UCB0SIMO	x				x		TB0-3/TA0-0	MOSI	magnetometer			MOSI	magnetometer	MOSI	magnetometer	MOSI	magnetometer	MOSI	magnetometer	MOSI	magnetometer	MOSI	magnetometer
32	P1.7	UCB0SOMI	x				x		TB0-4/TA1-0	MISO	magnetometer			MISO	magnetometer	MISO	magnetometer	MISO	magnetometer	MISO	magnetometer	MISO	magnetometer	MISO	magnetometer
33	P4.4	GPIO	x						TB0-5	shutup_en	ICP			shutup_en	ICP	shutup_en	ICP	shutup_en	ICP	shutup_en	ICP	shutup_en	ICP	shutup_en	ICP
34	P4.5	GPIO	x							trigger	sun 2			trigger	sun 2	trigger	sun 2	trigger	sun 2	trigger	sun 2	trigger	sun 2	trigger	sun 2
35	P4.6	GPIO	x							interrupt				interrupt		interrupt		interrupt		interrupt		interrupt		interrupt	
36	DVSS	DVSS																							
37	DVCC	DVCC																							
38	P2.7	GPIO	x							enable	magnettorquer	Start	sun 4			enable	magnettorquer	enable	magnettorquer					Start	sun 4
39	P2.3	ADC6	x		x	x	x		TA0-0	current	magnettorquer	CLK	sun 3			current	magnettorquer	current	magnettorquer					CLK	sun 3
40	P2.4	ADC7	x		x	x	x		TA1-0	temp sensor				temp sensor		temp sensor		temp sensor		temp sensor		temp sensor		temp sensor	
41	AVSS	AVSS																							
42	PJ.6	GPIO																							
43	PJ.7	GPIO																							
44	AVSS	AVSS																							
45	PJ.4	GPIO																							
46	PJ.5	GPIO																							
47	AVSS	AVSS																							
48	AVCC	AVCC																							

Lihtlitsents lõputöö reprodutseerimiseks ja lõputöö üldsusele kättesaadavaks tegemiseks

Mina, Aleksander Parelo,

1. annan Tartu Ülikoolile tasuta loa (lihtlitsentsi) enda loodud teose

Development of ESTCube-2 side panels

mille juhendajad on Hendrik Ehrpais ja Erik Ilbis

1.1. reprodutseerimiseks säilitamise ja üldsusele kättesaadavaks tegemise eesmärgil, sealhulgas digitaalarhiivi DSpace-is lisamise eesmärgil kuni autoriõiguse kehtivuse tähtaja lõppemiseni;

1.2. üldsusele kättesaadavaks tegemiseks Tartu Ülikooli veebikeskkonna kaudu, sealhulgas digitaalarhiivi DSpace´i kaudu kuni autoriõiguse kehtivuse tähtaja lõppemiseni.

2. olen teadlik, et punktis 1 nimetatud õigused jäävad alles ka autorile.
3. kinnitan, et lihtlitsentsi andmisega ei rikuta teiste isikute intellektuaalomandi ega isikuandmete kaitse seadusest tulenevaid õigusi.

Tartus, **20.05.2018**